SHAHBANDI, ALI, M.S. Exploration of interactions between commensal *Staphylococci* and methicillin-resistant *Staphylococcus aureus.* (2021)
Directed by Dr. Nadja B. Cech. 34 pp.

Methicillin-resistant *Staphylococcus aureus* (MRSA) is a multidrug-resistant superbug that causes infections in immunocompromised and immunocompetent individuals. This infection causes more than 300,000 infections and more than 10,000 deaths, with healthcare associated costs of over $1.7 Billion per year in the United States alone. Given the high morbidity and mortality for this pathogen, there is an urgent need to identify new treatment modalities against MRSA. One important step towards combating this infection is understanding the molecular interaction between commensal *Staphylococci* (those that live on healthy human skin) and MRSA. *Staphylococci* use a cell-density dependent regulatory system known as the quorum sensing accessory gene regulator system (*agr*). The *agr* system is also responsible for producing virulence factors that allow MRSA to proliferate on the host skin. This regulatory system's direct output is the auto-inducing peptide (AIP) molecule that is unique to each *Staphylococcus* strain. It is possible to detect the *agr* system's activity by measuring the concentration of the AIP molecule. Some commensal *Staphylococci* have shown inhibitory activity against the MRSA *agr* system in animal models.

This project aimed to study the molecular interaction between MRSA and the commensal strain *S. simulans*, *S. hominis*, and *S. warneri*. The AIP structures of the commensal strains were identified. The co-culture study showed that *S. simulans* inhibits the AIP production of MRSA; however, *S. hominins* and S. *warneri* did not induce a measurable impact on MRSA AIP production compared to the single culture of this species. Two previously identified growth indicator molecules of MRSA, aureusimine A and aureusimine B, were monitored in all co-culture samples of MRSA. The abundance

of these molecules in samples indicated that MRSA was growing in the co-culture samples of *S. simulans* even though the AIP production in these samples was being inhibited. Through untargeted metabolomics and utilization of selectivity ratio analysis, the increased abundance of features vs. time was analyzed in the single culture samples of MRSA and *S. simulans* and their co-cultures. Several (five) features were detected in the mass spectrometry data that were differentially expressed in the co-cultures versus monocultures. Future experiments are planned to identify the molecules associated with these features.

EXPLORATION OF INTERACTIONS BETWEEN COMMENSAL *STAPHYLOCOCCI*

AND METHICILLIN-RESISTANT *STAPHYLOCOCCUS AUREUS*

by

Ali Shahbandi

A Thesis Submitted to the
Faculty of the Graduate School at
The University of North Carolina at Greensboro
in Partial Fulfillment
of the Requirements for the Degree
Master of Science

Greensboro
2021

Approved by

_____
Committee Chair

To my family, for their continued support and encouragement, and to my wonderful professors for their inspirations. I could not have done it without you.

APPROVAL PAGE

This thesis, written by ALI SHAHBANDI, has been approved by the following

committee of the Faculty of the Graduate School at the University of North Carolina at

Greensboro.

       Committee Chair   _____

      Committee Members   _____

                         _____

_____
Date of Acceptance by Committee

_____
Date of Final Oral Examination

ACKNOWLEDGEMENTS

TABLE OF CONTENTS

LIST OF TABLES

LIST OF FIGURES

CHAPTER I

INTRODUCTION

Commensal bacterial species coat the human skin and mucosal surfaces. The skin is populated by the commensal bacterial genera *Staphylococcus, Streptococcus, Corynebacterium,* and *Propionibacterium.* Within the *Staphylococcus* genus, the most commonly isolated Gram-positive species are *S. epidermidis, S. hominis, S. haemolyticus, S. capitis, S. lugdunensis, and S. warneri.*[1-3] A pathogenic strain within the genus *Staphylococcus*, methicillin-resistant *Staphylococcus aureus* (MRSA)*,* causes infection in both immunocompromised and immunocompetent populations that are complicated to treat. According to the 2019 Antibiotic Resistance threats report by the Centers for Disease Control and Prevention, MRSA is responsible for more than 323,000 infections and more than 10,000 deaths per year in the United States, with an attributed healthcare cost of $1.7 billion.[4] One important step towards addressing this problem is understanding the extensive molecular interactions between beneficial commensal micro-organisms and pathogenic ones.

There is growing evidence that extensive interactions occur between commensal bacterial strains against MRSA.[5,6] This interaction is mediated by signaling molecules that can cause cross-inhibition across different species of *Staphylococci.*[7-9] This competitive interaction between MRSA and commensal species changes the pathogenesis of MRSA.[10-16] Understanding the commensal and MRSA interaction dynamic is crucial

because it can shed light on the mechanisms of MRSA pathogenicity and present possible strategies to develop new treatment modalities.

Cell-to-cell communication in all *Staphylococci* is accomplished through the quorum sensing system, referred to as the accessory gene regulator (*agr*) system (Figure 1).[17] The *agr* system in *Staphylococci* plays a role in cell-to-cell communication. This developed mode of communication system has also been associated with the regulation of colonization and virulence factors. The *agr* system is activated by a cell density-dependent signaling molecule autoinducing peptide (AIP). As bacteria proliferate, the concentration of the AIP molecule increases outside of the cell until it reaches a specific concentration and binds to a histidine kinase receptor, AgrC, on the surface of the bacterial cell. This binding activates the transcription factor, AgrA, that binds to P2 and P3 promoters. This binding generates an *agr* locus that produces two primary transcripts, RNAII and RNAIII.[18–20] Four proteins are encoded by the P2 operon that generates the *agr*-sensing mechanism. The transmembrane protein AgrB is involved in processing the AgrD product into a peptide, AIP secretion, and the formation of a cyclic thiolactone bond between an internal cysteine and the carboxyl terminus modifies the AIP molecule.[21] This *agr* system is positively associated with human MRSA infection of the skin and soft tissue.[16,22,23] It has also been shown that innate immunity against experimental MRSA skin infection requires active suppression of *agr* signaling.[1,17,24,25] Therefore, the AIP molecule can be used to track the activity of the *agr* system based on the produced quantity.[26] An important goal of this study is to track the quantity of the AIP molecule of MRSA in single and co-cultures samples with commensal strains *S. simulans, S. warneri,* and *S. hominis.*
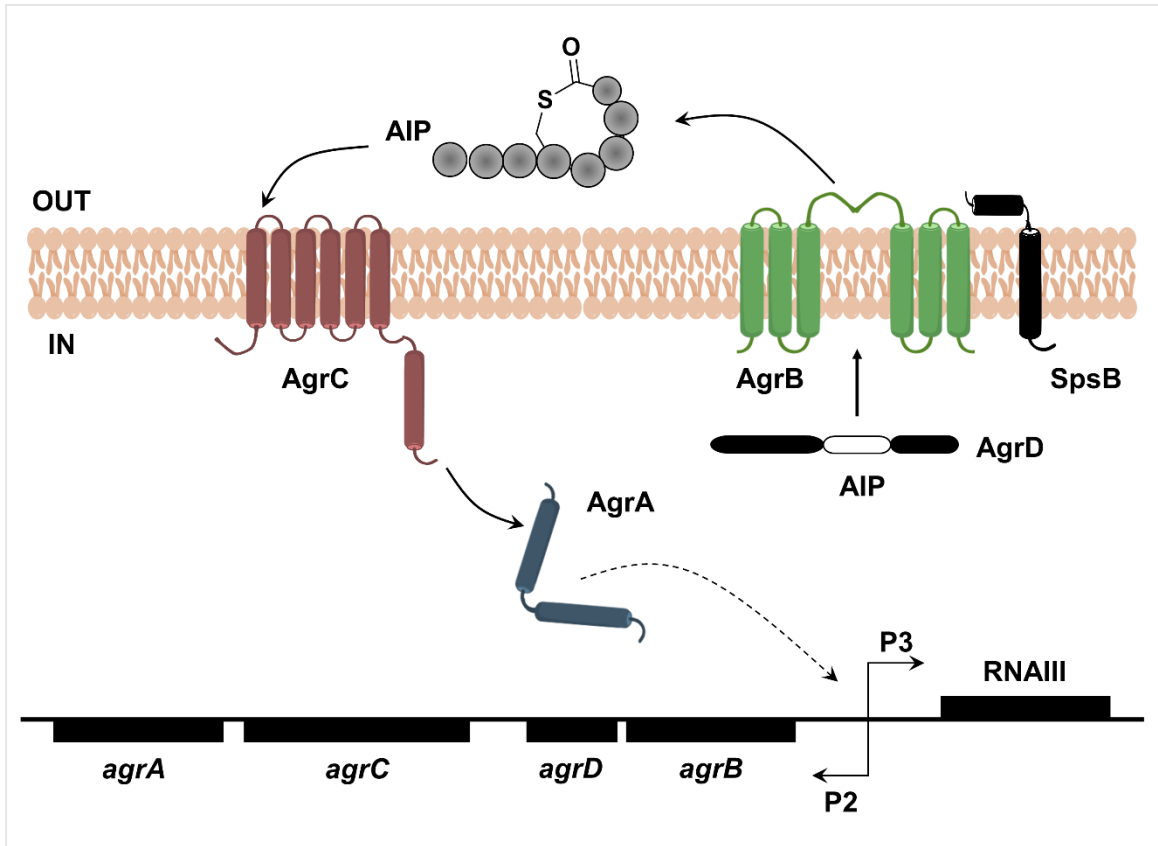
Figure 1. Schematic of the *agr* system in MRSA*.* The AIP signaling molecule are secreted and processed by an AgrB-dependant process. Binding of AIP to AgrC results in phosphotransfer to AgrA, which induces transcription at the P2 and P3 promoters of the agr operon and RNA III, respectively.[17]

In recently published results with our collaborators,[6] *S. simulans* AIP, showed inhibitory activity against MRSA in murine models. In this study, BALB/c mice were intradermally co-infected with equal colony forming units (CFU) of MRSA and *S. simulans*. Mice co-infected with *S. simulans* and MRSA had significantly decreased dermonecrotic lesions over the experimental period (P 0.0001) compared to mice infected with MRSA alone. Furthermore, co-infected mice were healthier compared to mice that were infected by MRSA alone. These results are demonstrated by mouse weight changes. These results show that when *S. simulans* competes with MRSA, tissue damage is significantly reduced.

3

In vivo studies testing the synthetic AIP from *S. simulans* (AH4549) against BLAB/c mice infected with MRSA showed diminished skin injury. The results from this study demonstrate that *S. simulans* (AH4549) AIP is a quorum sensing inhibitor of MRSA in vivo, and it can protect the host from MRSA induced skin injury.

Recently, metabolites not associated with the *agr* system have been used to track the growth of MRSA. Production of aureusimines by MRSA has been previously reported,[27] and the production of these molecules are dependent on the ausAB operon, which encodes a non-ribosomal peptide synthetase (ausA) and a 4′-phosphopantetheinyl transferase (ausB). In early reports, it was suggested that aureusimines were virulence regulators in MRSA;[28] however, further studies showed that the observed virulence inhibitory activity was due to a secondary mutation in the SaeR5 two-component system.[29] Therefore, the biological roles of aureusimines is unknown. In this study, we utilized aureusimines as indicators of MRSA growth based on a method previously developed by Jones, et al.[27]

In this study, the *agr* system regulating peptide of the pathogen MRSA was quantified in the single and co-culture conditions with commensal bacterial strains *S. simulans, S. warneri,* and *S. hominis.* The commensal AIP was also quantified in the single and co-culture conditions to gain insight into the inhibitory activity of commensal strains against MRSA. The relative abundance of known metabolites produced by MRSA, such as the aureusimines, was also monitored to track the growth of MRSA in the co-culture conditions. Finally, the samples were subjected to untargeted metabolomics to screen for unique molecules that are either upregulated or downregulated in the co-culture conditions.

CHAPTER II

METHODS

Bacterial Growth and Filtration

Single colonies (Figure 2-1) of the strains *S. hominis* (AH5011), *S. simulans* (AH4549), and *S. warneri* (AH4548) were inoculated in 3 mL of tryptic soy broth (TSB) (Figure 2-2) separately and incubated at 37°C with shaking of 250 rpm for 24 hours (Figure 2-3). For co-culture samples, 150 µL of a commensal strain and 150 µL of MRSA seed culture were added to 30 mL of fresh TSB to make 1:200 (culture/TSB) dilution of each strain. The single cultures were prepared by transferring 150 µL of the seed culture into 30 mL of fresh TSB to make the 1:200 dilution samples. All samples were then incubated at 37°C with shaking of 250 rpm for up to 18 hours. Samples were collected at 2, 4, 6, 12, and 18 hours and transferred to different sections of the 96 well pla te for each timepoint to measure OD_{600} using a Synergy H1 Plate Reader (Figure 2-5). Each sample was vacuum filtered in a Multiscreen-GV Filter plate, 0.22 µm pore size hydrophilic PVDF membrane (Figure 2-6). All filtered samples were injected into the ultrahigh-performance liquid chromatography (UPLC) system (Waters Corporation) coupled to a Q Exactive Plus hybrid quadrupole-Orbitrap mass spectrometer (MS) (Thermo Fisher Scientific) for separation (Figure 2-7 and Figure 2-8, respectively).

Figure 2. Workflow for the experimental methods of bacterial cultures.

AIP Identification

All samples were analyzed using UPLC-MS. A 7-µL injection of each sample was eluted from an Acquity UPLC BEH C18 1.7-m, 2.1 by 50 mm column (Waters Corporation) at a flow rate of 0.3 mL/min using a 10-minute binary gradient of water (Optima LC-MS grade) with 0.1% formic acid and acetonitrile (Optima LC-MS grade) with 0.1% formic acid. Mass spectra were collected using two scan events utilizing positive-mode electrospray ionization, a full-scan event over a mass range of 300 to 2,000 at a resolving power of 35,000, and a data-dependent tandem mass spectrometry (MS/MS) scan event selecting the calculated *m/z* values of the predicted AIPs. The mass spectrometer was operated using the following settings: capillary temperature set at 300°C, S-Lens radio frequency (RF) level set at 80, spray voltage set at 4.0 kV, sheath gas flow set at 50, and auxiliary gas flow set at 15. Precursor ions detected in the full scan were selected, with an isolation window of 4 Da, and subjected to high-energy collision dissociation (HCD) fragmentation at a normalized collision energy of 25. Synthetic standards for each the predicted AIP

molecule were purchased from AnaSpec, EGT (Fremont, CA), and subjected to the same UPLC-MS analysis. The accurate mass, retention time, and fragmentation patterns for synthetic standards were compared to those of putative AIP ions in spent media to confirm AIP structures.

Quantitative Analysis of AIPs

The AIP concentration of the pathogen MRSA and commensal strains *S. simulans, S. warneri,* and *S. hominis* were calculated by plotting the AIP molecule's average peak area as a function of the known concentration of the synthetic standard. The synthetic standards of the AIP molecules were acquired from Anaspec EGT (Fremont, CA) and prepared by serial dilution of a 4.00 µM sample eight times to the minimum concentration of 0.03 µM. The standards were all combined in fresh bacterial growth medium TSB and analyzed via UPLC-MS. The MS^2 fragmentation and retention of each AIP synthetic standard were compared to the suspected AIP molecule in each single and co-culture sample spent medium.

Untargeted Metabolomics

The data collected from the UPLC and MS were analyzed, deconvoluted, deisotoped, and aligned using MZmine 2.53 software. These data were then exported to MS Excel, where blanks and the background noise were manually removed from the sample mass spectral profile. The relative standard deviation (RSD) of the peak area for each feature in each culture triplicate was calculated, and features with an RSD value of great than 25% were deleted.

Selectivity Ratio Analysis

        The UPLC-MS filtered data were subjected to selectivity ratio analysis.[27,30] The selectivity ratio was employed to identify features that increased in abundance over time in the individual and co-cultured bacterial samples. Selectivity ratio analysis was performed using the Sirius 11.5 (Pattern Recognition System AS, Bergen, Norway). Selectivity ratio analysis is a strategy to reduce complex mass spectrometric data sets to simplified models that allow the identification of features that correlate with a particular dependent variable, in this case, growth time.

CHAPTER III

RESULTS AND DISCUSSION

Commensal *Staphylococcus* AIP Identification

Cell-to-cell communication in all *Staphylococcus* strains occurs via the *agr* system. This method of communication regulates colonization and virulence factor production.[17] Quorum sensing in the *Staphylococci* is mediated by the AIP signaling molecule. Most *Staphylococcus* species and subspecies produce a unique AIP molecule. It is essential to identify the structure of the AIP signaling molecule in commensal and pathogenic strains within this genus so that AIP production can be used to track the activity of the *agr* system.

To identify the AIP structures of commensal species *S. warneri*, *S. hominis,* and *S. simulans,* published gene sequence data for AgrD was used in combination with the mass spectrometric analysis of spent media. All of the identified AIP molecules are cyclic peptides that contain a five amino acid thiolactone ring. This thiolactone ring results from the linkage of the sulfhydryl group of the cysteine and the α-carbonyl group of the C-terminus. For *S. warneri,* the singly charged, protonated molecular ion ($[M+H]^+$ 960.3914) of the AIP molecule was detected. This molecule is a 9-amino-acid AIP (YSPCTNFF) with calculated and measured *m/z* values of 960.3927 and 960.3914 (mass error 1.4 ppm), respectively. Synthetic *S. warneri* AIP was used for additional validation and characterization. Liquid chromatography-mass spectrometry (LC-MS) analysis of the synthetic AIP showed matching retention time, *m/z* value, and fragmentation patterns with the native AIP structure identified in each *S. warneri* isolate spent media (Figure 3).

The *S. simulans* AIP was identified by detecting an ion with *m/z* 1036.5302 in the spent media. This ion corresponds to the 9-amino-acid AIP (KYNPCLGFL) that was detected with calculated and measured *m/z* values of 1,036.5286 and 1,036.5302 (mass error 1.6 ppm), respectively (Figure 4).[6] The identification of the *S. hominis* AIP was possible by detecting the [M+H]$^+$ ion with *m/z* 957.4140. This ion corresponds to the 9 amino acid AIP (TINTCGGYF) with calculated and measured *m/z* values of 957.4140 and 957.4132 (mass error 0.84 ppm), respectively. The MS/MS fragmentation of the selected ions was compared to a synthetic standard to confirm the sequence of the AIP molecules (Figure 5).

Figure 3. Identification and validation of *S. warneri* (AH4548) AIP ([M+H]+ 960.3927). Retention comparison of the detected ion in spent medium and the AIP standard (A). The structure of the AIP molecule was confirmed using MS/MS analysis of the spent medium and the synthetic AIP standard (B). The confirmed amino acid sequence identified is YSPCTNFF and the structure of this molecule is shown above with the labeled cleavage sites. The colors on the structure correspond to the mass spectrum fragments shown.
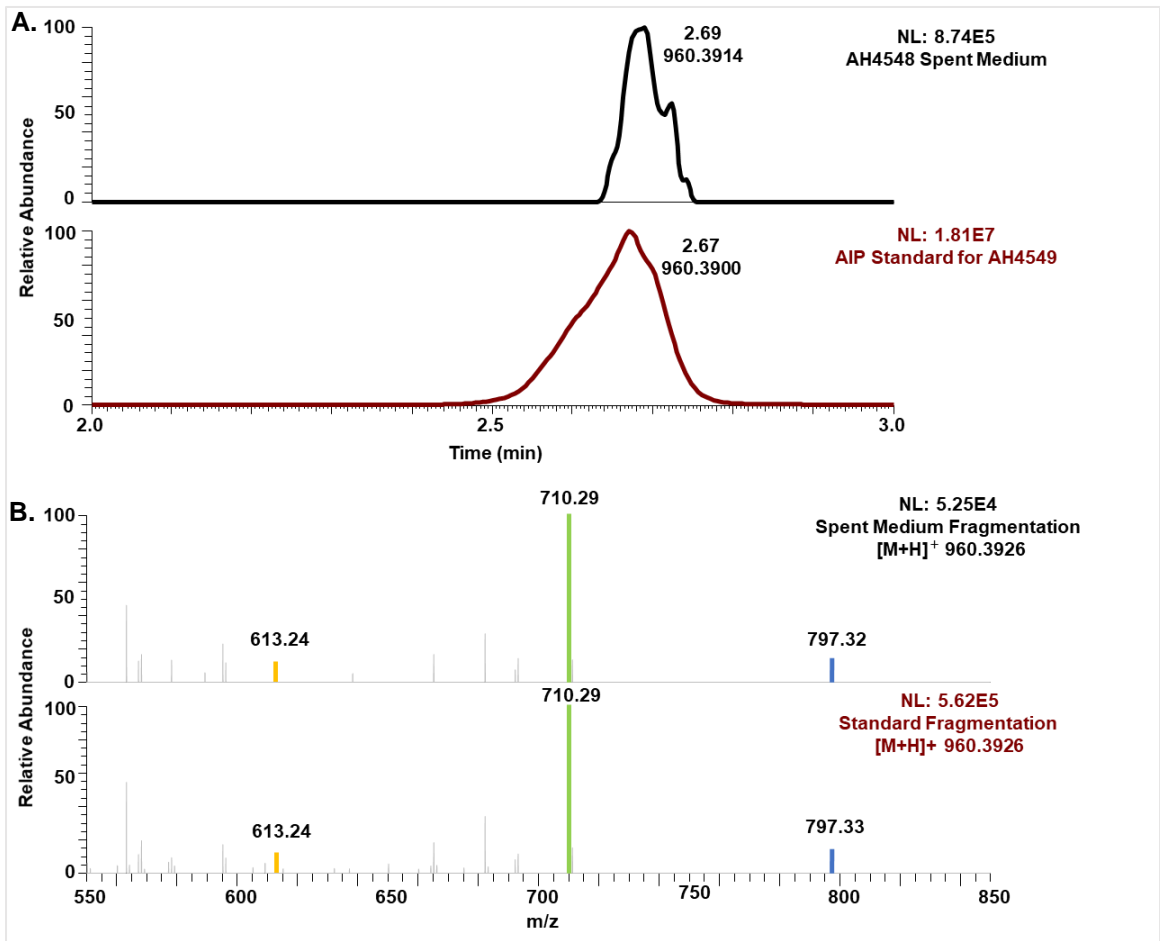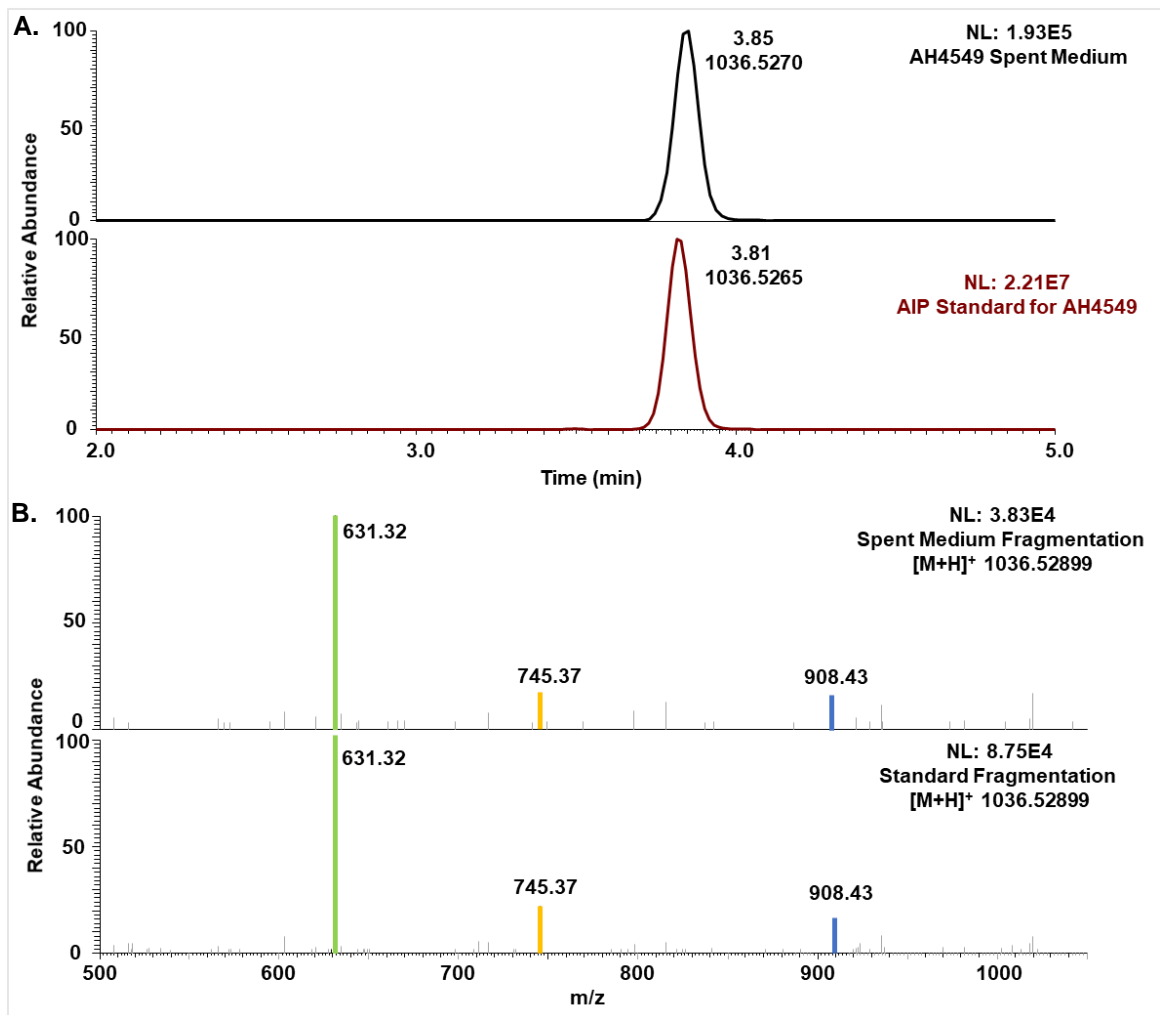
Figure 4. Identification and validation of *S. simulans* (AH4549) AIP ([M+H]+ 1036.5285). Retention comparison of the detected ion in spent medium and the AIP standard (A). The structure of the AIP molecule was confirmed using MS/MS analysis of the spent medium and the synthetic AIP standard (B). The confirmed amino acid sequence identified is KYNPCLGFL and the structure of this molecule is shown above with the labeled cleavage sites. The colors on the structure correspond to the mass spectrum fragments shown.
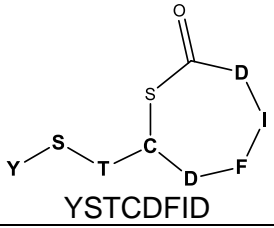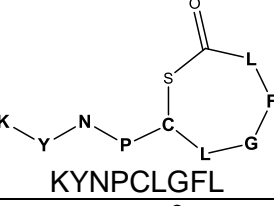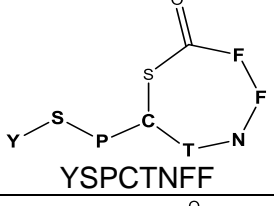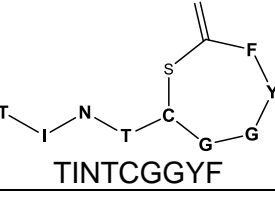
Figure 5. Identification and validation of *S. hominis* (AH5011) AIP ([M+H]+ 957.4140). Retention comparison of the detected ion in spent medium and the AIP standard (A). The structure of the AIP molecule was confirmed using MS/MS analysis of the spent medium and the synthetic AIP standard (B). The confirmed amino acid sequence identified is TINTCGGYF and the structure of this molecule is shown above with the labeled cleavage sites. The colors on the structure correspond to the mass spectrum fragments shown.
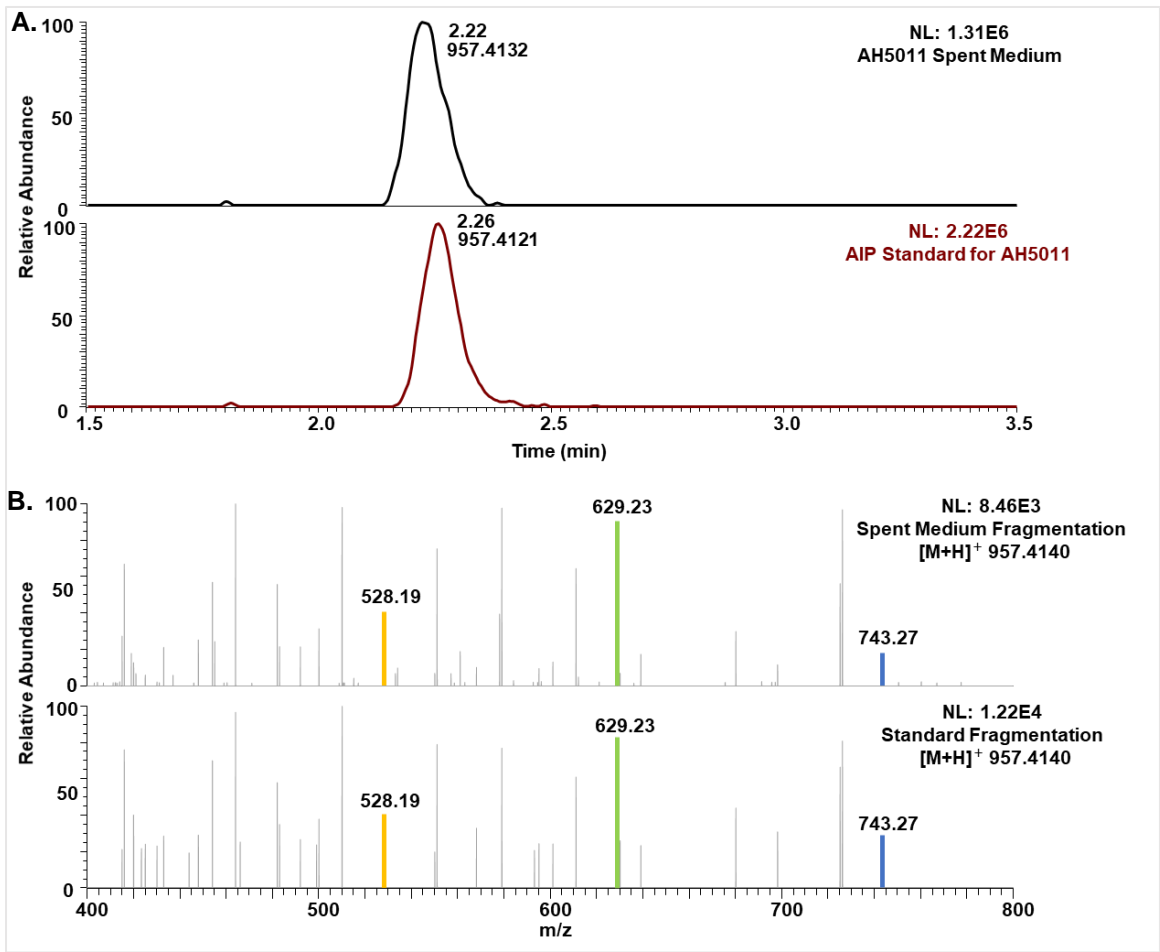
This method was also applied to detect the AIP molecule for MRSA, and the identified sequence agreed with previously published results.[31] The [M+H]+ 961.3774 ion of this AIP molecule corresponds to the 9-amino-acid peptide YSTCDFID with calculated and measured *m/z* of 961.3798 and 961.3774 (mass error 2.50 ppm), respectively. Table 1 shows the identified structure for all the bacteria strains in this study.

Table 1. Bacterial strains with identified AIP sequence

Species	Strains name	AgrD Sequence	AIP Structure	Description
Methicillin-resistant *Staphylococcus aureus*	AH1263	NIAAYSTCDFID	YSTCDFID	WT USA300 LAC MRSA (*agr* type I)
Staphylococcus simulans	AH4549	NLAKYNPCLGFL	KYNPCLGFL	ATCC Strain 27848/ MK148
Staphylococcus warneri	AH4548	FVAGYSPCTNFF	YSPCTNFF	ATCC Strain 27836/ AW25
Staphylococcus hominis	AH5011	NIATINTCGGYF	TINTCGGYF	Atopic Dermatitis skin Isolate

Co-Culture Analysis of Commensal Strains with MRSA

Bacterial growth is typically monitored by measuring the optical density of the solution at 600 nm (OD_{600}). To monitor the growth of the bacterial cultures, OD_{600} readings were done at 2-hour intervals for the first 6 hours and at 12 hours and 18 hours. All samples showed an increase in OD_{600} of co-culture samples compared to the single cultures (Figure 6). In the co-culture setting, however, it will be difficult to conclude which bacterium is responsible for the observed increase in turbidity, and the OD_{600} readings

should be interpreted as a measure of the overall growth for both bacterial strains combined.
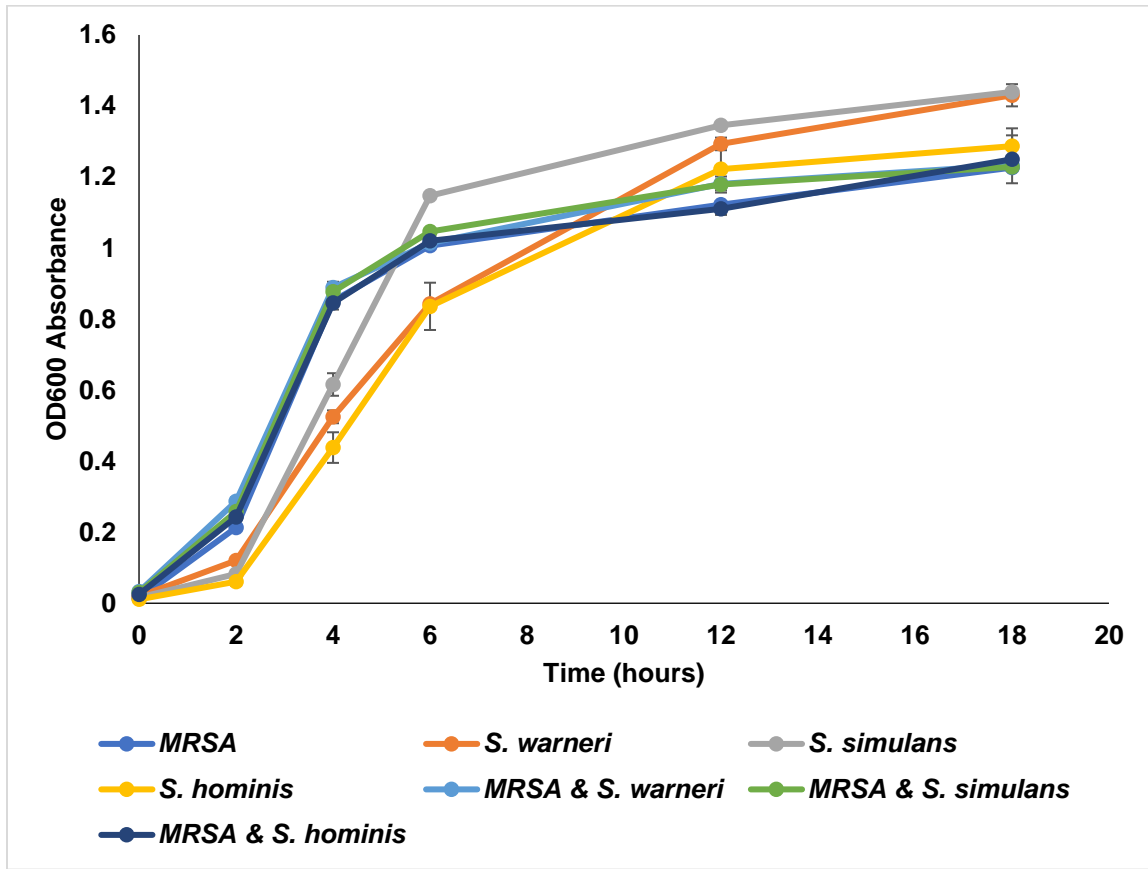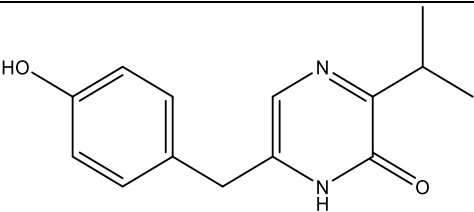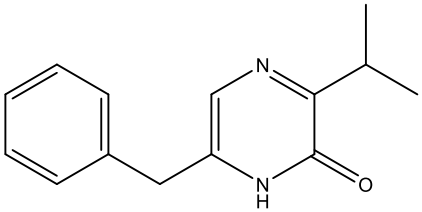

Figure 6. Growth curve for MRSA*, S. warneri, S. simulans,* and *S. hominis* single cultures and each commensal co-culture with MRSA. Evaluation of growth effect for each bacterial single culture compared to the co-culture samples with MRSA. Growth samples were collected over an 18 hour time period at 2 hour, 4 hour, 6 hour, 12 hour, and 18 hour timepoints.

Table 2. Aureusimine A and Aureusimine B

Name	Structure	[M+H]+ ion *m/z*
Aureusimine A		245.1285
Aureusimine B		229.1335

To track the presence of MRSA in the co-culture sample, the relative abundance of two metabolites aureusimine A and aureusimine B in the MRSA single and co-culture samples was monitored. The function of aureusimine A and B (Table 2) is still the subject of debate; however, aureusimine B was reported to be associated with MRSA growth independent of the *agr* system.[27] A similar observation is made in the results of this experiment for aureusimine B. Figures 7 shows the peak area as a function of time for aureusimine B in the single culture of MRSA as well as the co-culture of this strain with *S. hominis, S. simulans,* and *S. warneri.* The abundance of aureusimine B in the single culture of MRSA is higher compared to the co-culture samples. This decreased in abundance is potentially due to competition of MRSA with each commensal strain. However, these data show that although there is competition among MRSA and commensal strains, MRSA growth is still present in the co-culture samples. Similar observations are made in Figure 8, where the relative abundance of aureusimine A is

16

analyzed in MRSA single culture and when this strain is co-cultured with commensal strain. Further supporting the claim that MRSA is growing in the co-culture samples.
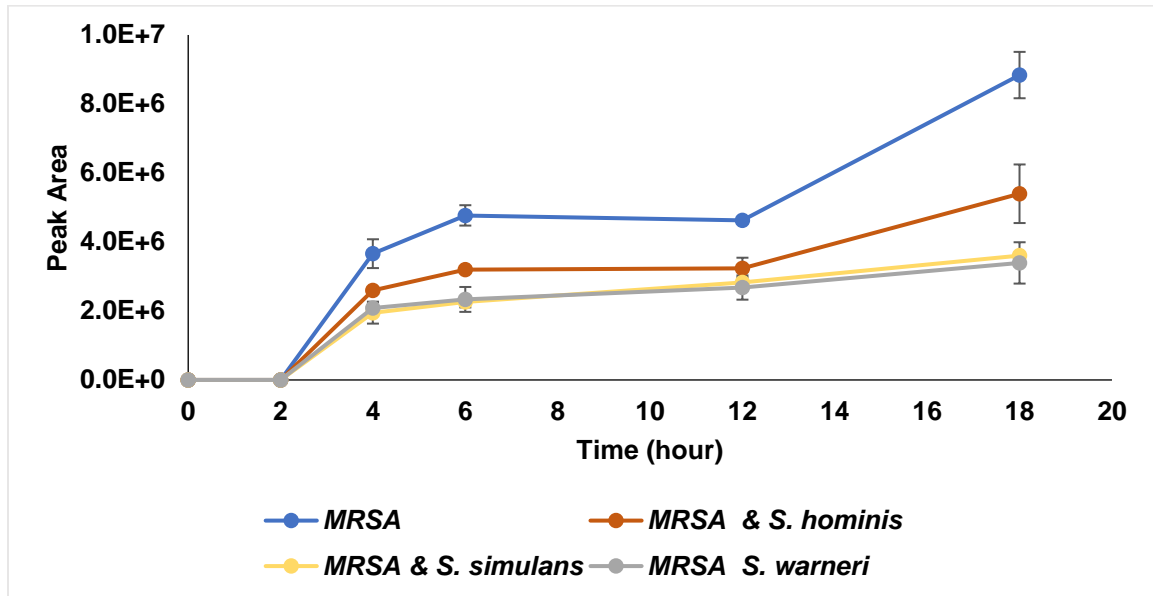

Figure 7. Abundance (as measured by UPLC-MS peak area) over time of aureusimine B (*m/z* 229.1335) in MRSA single cultures and co-cultures of MRSA with *S. hominis, S. simulans,* and *S. warneri.*
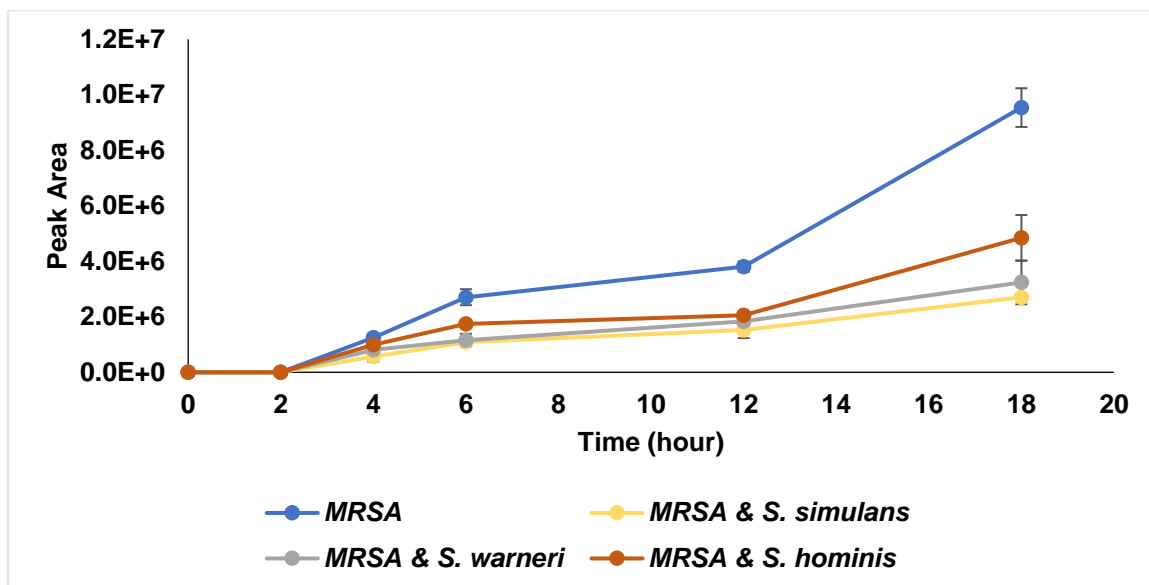
Figure 8. Abundance (as measured by UPLC-MS peak area) over time of aureusimine A (*m/z* 245.1285) in MRSA single culture and co-cultures of MRSA with *S. hominis, S. simulans,* and *S. warneri.*

AIP concentration was also determined in the single and co-culture samples (Table 3). The concentration of the AIP molecule for MRSA corresponds to the ion detected at *m/z* 961.3798 was calculated by plotting the average peak area as a function of known concentrations of the AIP molecule from a synthetic standard ranging from 0.12 μM to 2.00 μM. In the co-culture samples of *S. simulans* and *S. hominis* with MRSA, the MRSA AIP molecule's quantity was consistent with the single culture of MRSA. This means the *agr* system in MRSA was not inhibited. However, the quantity of the MRSA AIP molecule in the co-culture of MRSA and *S. simulans* was below the limit of detection (LOD). Figure 9 shows the graphical representation of the reported values in Table 3. The quantity of the MRSA AIP molecule was plotted as a function of the time for each co-culture sample as well as the control single culture of MRSA. The concentration of the MRSA AIP molecule is below the LOD; however, as aureusimine A and aureusimine B data indicated (Figure

7 and Figure 8, respectively), MRSA is still growing in the co-culture samples with *S. simulans.* From this data, we can conclude that the virulence in MRSA, as indicated by the AIP molecule, is being inhibited even though MRSA is growing.

Table 3. Hourly *MRSA* AIP I (*m/z* 961.3798) concentration ± Standard Deviation (SD) in single and co-culture samples with the LOD and LOQ of 0.065 and 0.197, respectively.

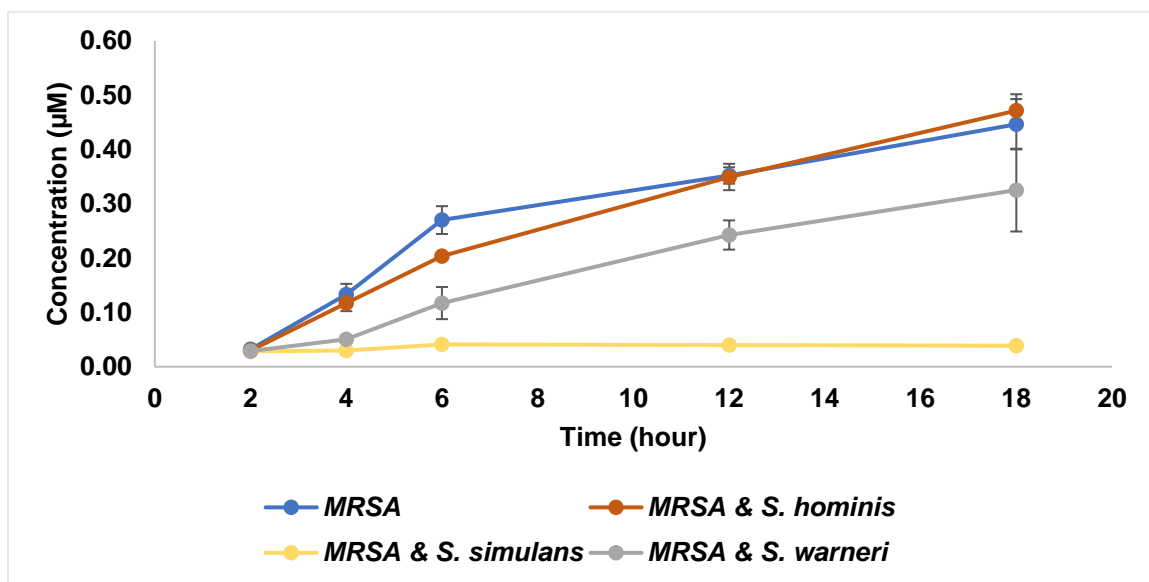| Time (Hour)	MRSA AIP Concentration (µM)			
	MRSA	**MRSA & *S. simulans***	**MRSA & *S. warneri***	**MRSA & *S. hominis***
2	Below LOD	Below LOD	Below LOD	Below LOD
4	0.133 ± 0.02	Below LOD	Below LOD	0.117 ± 0.01
6	0.270 ± 0.03	Below LOD	0.117 ± 0.03	0.204 ± 0.01
12	0.352 ± 0.02	Below LOD	0.243 ± 0.03	0.349 ± 0.02
18	0.447 ± 0.05	Below LOD	0.325 ± 0.08	0.472 ± 0.03

Figure 9. Quantitative analysis of the AIP I (*m/z* 961.3798) in the single culture of MRSA and when this strain was co-cultured with *S. warneri*, *S. hominis,* and *S. simulans.* The limit of the detection and limit of quantification for the AIP was calculated to be 0.065 µM and 0.197 µM respectively.

The concentration of each commensal AIP was calculated in the single culture as well as the co-culture samples with MRSA (Tables 4, 5, and 6). The production of *S. simulans, S. warneri,* and *S. hominis* AIPs were inhibited in all co-culture samples with MRSA. The inhibition of the commensal AIP production in the co-culture samples may be due to the ability of MRSA to inhibit the *agr* system in these commensal strains. The lack of commensal AIP detection could also be due to the lack of growth in the co-culture samples due to the presence of MRSA; however, they are currently no indicator molecules to track the growth of these commensal *Staphylococcus* strains.

Table 4. Hourly *S. simulans* AIP concentration $\pm$ SD. The LOD and LOQ of 0.085 µM and 0.256 µM, respectively.

Time (Hour)	*S. simulans* AIP Concentration (µM)	
	S. simulans	MRSA & *S. simulans*
2	Below LOD	Below LOD
4	Below LOD	Below LOD
6	0.134 $\pm$ 0.00	Below LOD
12	0.189 $\pm$ 0.00	Below LOD
18	0.211 $\pm$ 0.02	Below LOD

Table 5. Hourly *S. warneri* AIP concentration $\pm$ SD. The calculated LOD and LOQ of 0.095 μM, and 0.289 μM, respectively.

Time (Hour)	*S. warneri* AIP Concentration (μM)	
	S. warneri	MRSA & *S. warneri*
2	Below LOD	Below LOD
4	Below LOD	Below LOD
6	Below LOD	Below LOD
12	0.102 ± 0.01	Below LOD
18	0.117 ± 0.01	Below LOD

Table 6. Hourly *S. hominis* AIP concentration $\pm$ SD in single and co-culture samples. The calculated LOD and LOQ of 0.126 μM, and 0.380 μM, respectively.

Time (Hour)	*S. hominis* AIP Concentration (μM)	
	S. hominis	MRSA & *S. hominis*
0	Below LOD	Below LOD
2	Below LOD	Below LOD
4	Below LOD	Below LOD
6	Below LOD	Below LOD
12	0.356 ± 0.03	Below LOD
18	0.488 ± 0.03	Below LOD

Untargeted Metabolomics

Using untargeted metabolomics, we aimed to find upregulated and downregulated features in the single culture of MRSA, *S. simulans*, and the co-culture of these two strains. Selectivity ratio analysis was conducted to identify features that increased abundance in the bacterial cultures as a function of time. The features with the highest selectivity ratio are observed to increase in abundance with growth. In the MRSA selectivity ratio plot (Figure 10), the AIP molecule with the *m/z* of 961.3774 and retention time of 4.33 minutes is shown in this plot, as well as 3 unknown molecules. The features shown in gray are components of the growth medium or features that were identified across all bacterial strains. In the SR plot of *S. simulans,* the $[M+2H]^{2+}$ of the AIP molecule with the *m/z* of 518.7667 and retention time of 3.78 was observed. An unknown molecule was also identified in this sample with the $[M+3H]^{3+}$ of 1549.151 and a retention time of 8.02 minutes (Figure 11). In the co-culture selectivity ratio plot, the unknown molecule reported in the MRSA single culture was observed again. This molecule has an $[M+H]^{+}$ of 735.4073 and a retention time of 3.20 minutes (Figure 12).

Figure 10. Selectivity Ratio plot of MRSA samples. The plot was constructed using average peak areas for triplicate samples of the time course experiment. Samples were collected after 2, 4, 6, 12, and 18 hours. The selectivity ratio is based on the growth time.

Figure 11. Selectivity Ratio plot of *S. simulans* co-culture samples. The plot was constructed using average peak areas for triplicate samples of the time course experiment. Samples were collected after 2, 4, 6, 12, and 18 hours. The selectivity ratio is based on the growth time.

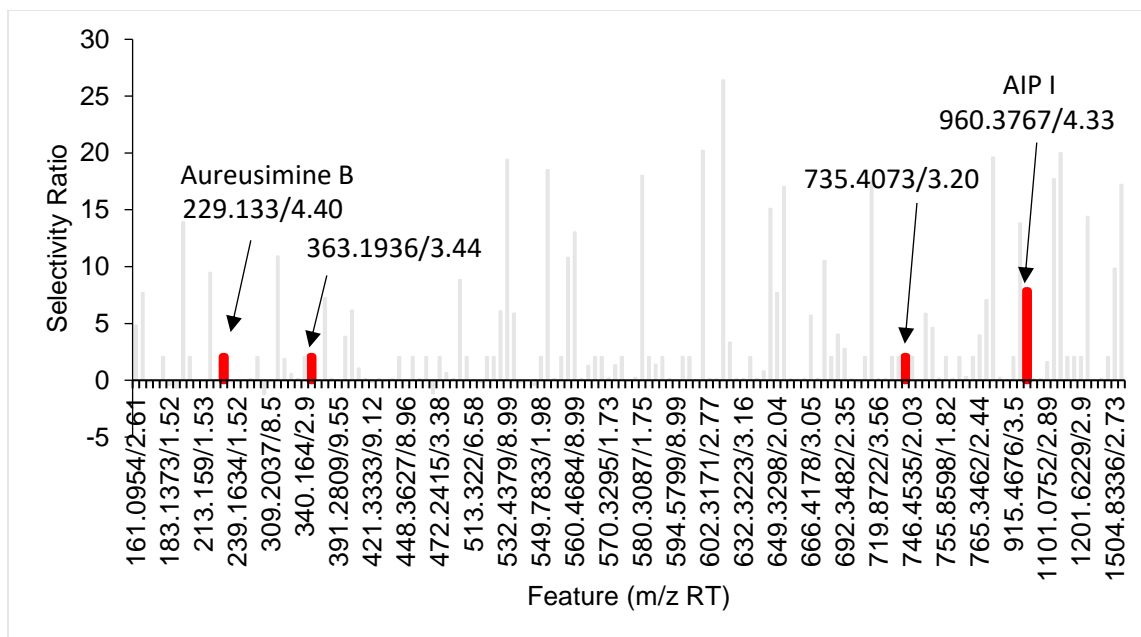**Figure 12.** Selectivity Ratio plot of MRSA & *S. simulans* co-culture samples. The plot was constructed using average peak areas for triplicate samples of the time course experiment. Samples were collected after 2, 4, 6, 12, and 18 hours. The selectivity ratio is based on the growth time.
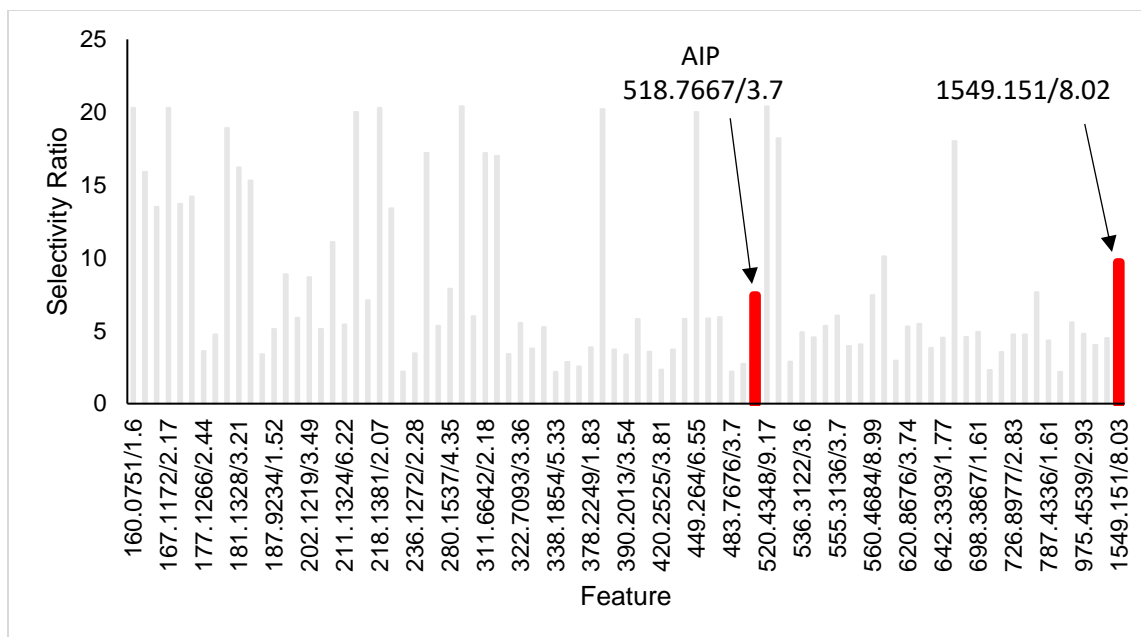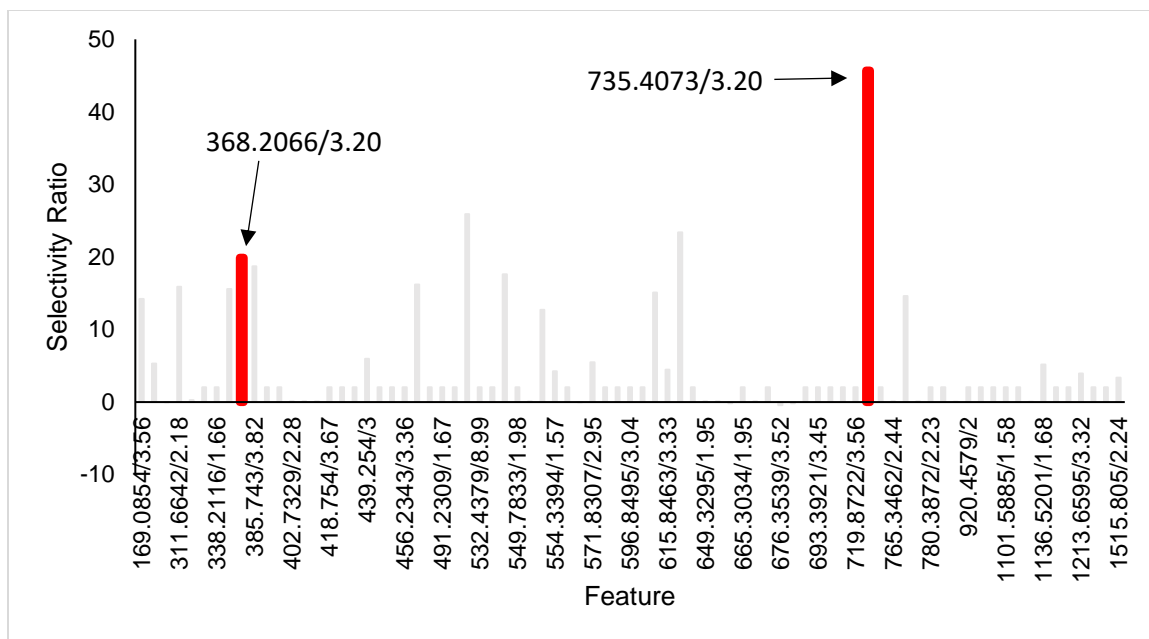
Abundance of the Unique Features from the Selectivity Ratio Plots

Given the diminished AIP concentration of MRSA and *S. simulans* in the co-culture samples, the peak area of the unique features identified (Table 7) from the selectivity ratio plots were used for relative abundance in different bacteria cultures as a function of growth time in hours (Figures 13-17). The ion with the *m/z* 363.1936 and the retention time of 3.44 minutes is identified in the MRSA single culture as well as the co-culture triplicate samples with *S. simulans.* As the relative concentration of this ion suggests, there is a minor difference between the detected concentration of this ion in MRSA single culture and the co-culture with *S. simulans* (Figure 13)*.* The $[M+2H]^{2+}$ ion 368.2066 with the retention time of 3.2 minutes (Figure 14) shows an increased relative concentration in the

25

co-culture sample. The [M+H]$^+$ ion 735.4073 with the retention time of 3.20 minutes (Figure 15) is suspected to be the singly charged ion of *m/z* 368.2066.

Table 7. Unique features identified from the selectivity ratio plots

ID	Feature (*m/z*)	RT	Sample	Ion Type
1	229.133	4.40	MRSA	[M+H]$^+$
2	363.1936	3.44	MRSA	[M+H]$^+$
3	735.4073	3.20	MRSA & *S. simulans*	[M+H]$^+$
4	368.2066	3.20	MRSA & *S. simulans*	[M+2H]$^{2+}$
5	511.3118	3.76	MRSA	[M+H]$^+$
6	1549.151	8.03	*S. simulans*	[M+3H]$^{3+}$

The singly charged ion with *m/z* 368.2066 has a calculated [M+H]$^+$ of 735.4054 compared to the detected *m/z* 735.4073 (mass error 2.6 ppm). The [M+H]$^+$ of 511.3118 is detected in the MRSA single culture as well as the co-culture with *S. simulans* (Figure 16). This ion shows an increased abundance in the co-culture samples compared to the single cultures of *S. simulans* and MRSA. The [M+3H]$^{3+}$ ion 1549.151 is detected in the *S. simulans,* and the abundance of this ion is significantly reduced compared to the co-culture samples of *S. simulans* with MRSA (Figure 17).

Figure 13. Abundance (as measured by UPLC-MS peak area) over time of the singly charged ion with *m/z* 363.1936 and retention time of 3.44 minutes.

Figure 14. Abundance (as measured by UPLC-MS peak area) over time of the doubly charged ion with *m/z* 368.2066 and retention time of 3.20 minutes.

Figure 15. Abundance (as measured by UPLC-MS peak area) over time of the singly charged ion with *m/z* 735.4073 with the retention time of 3.20 minutes.
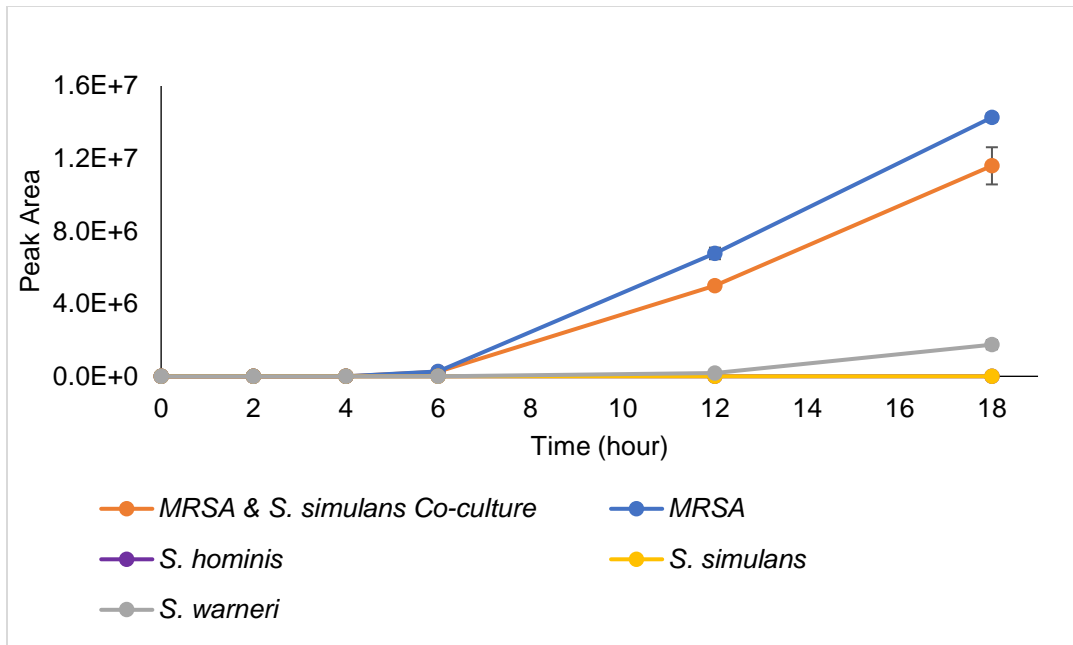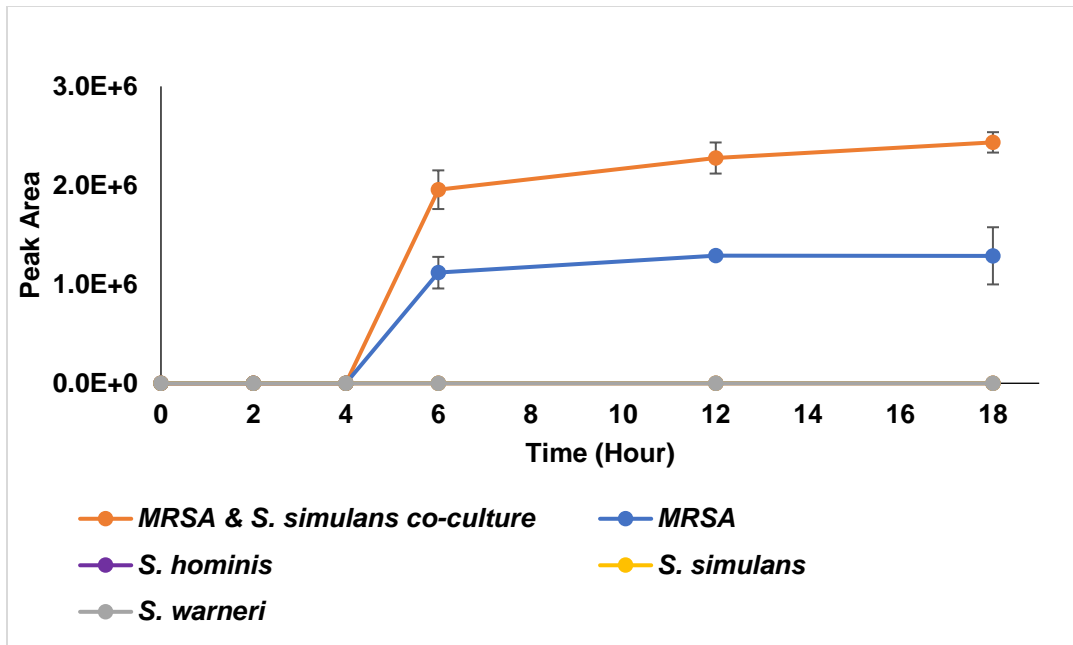
Figure 16. Abundance (as measured by UPLC-MS peak area) over time of the singly charged ion with *m/z* 511.3118 and retention time of 3.76 minutes.
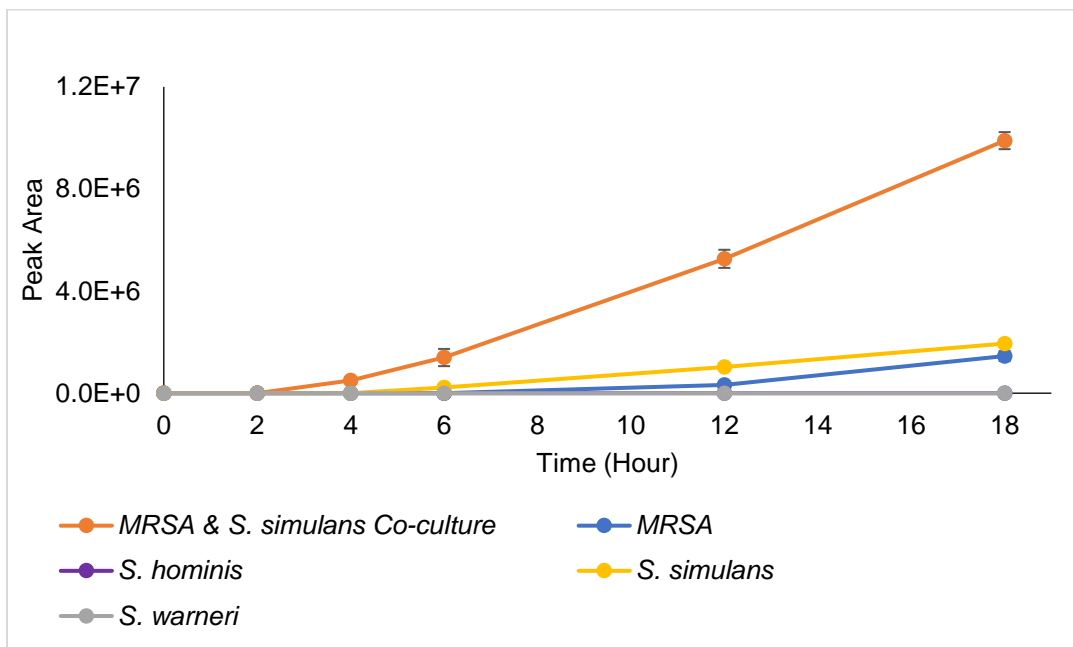
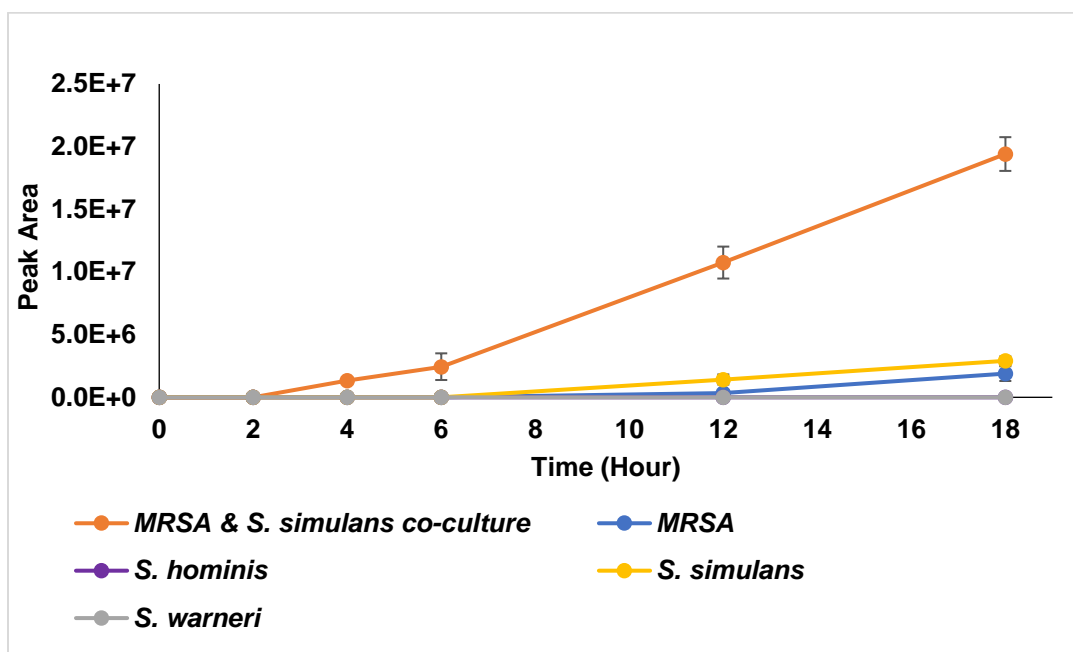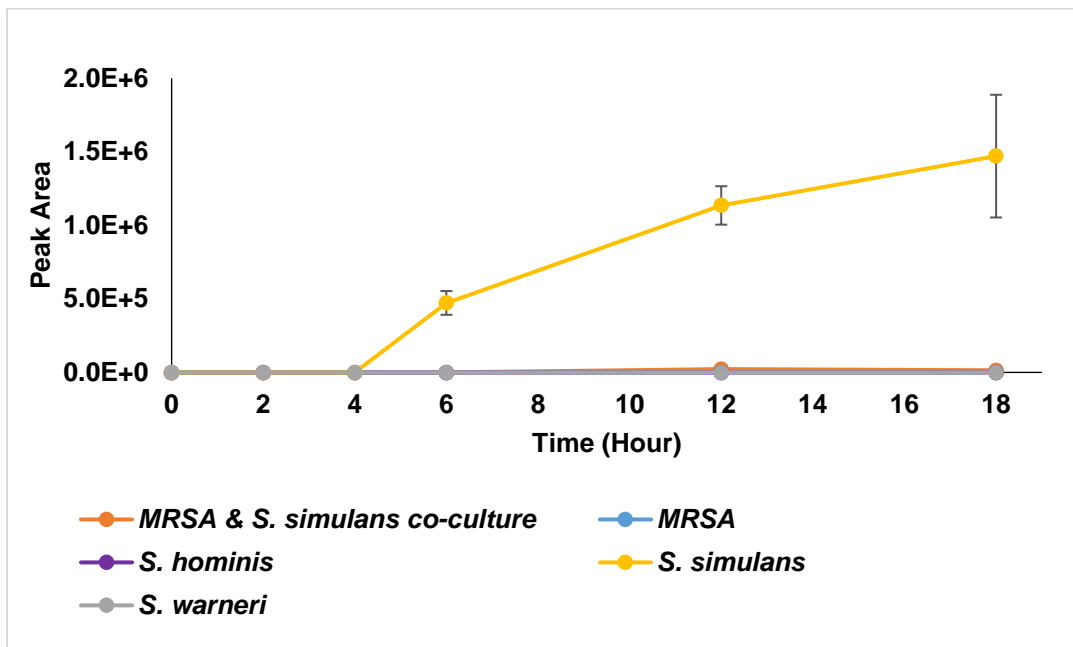

Figure 17. Abundance (as measured by UPLC-MS peak area) over time of the triply charged ion with *m/z* 1549.151 and the retention time of 8.02 minutes.

Based on a recent literature search, none of the ions shown in figures 13-17 appear to correspond to compounds that have been previously characterized from the bacterial strains under investigation. It is essential to characterize the structure of these detected molecules by isolating them as pure compounds. The pure compound from the complex mixture can be attained by using a flash chromatography technique. Each pure compound can then be further characterized, and structures elucidated using tandem mass spectrometry and nuclear magnetic resonance (NMR) spectroscopy.

CHAPTER IV

CONCLUSION

In the targeted metabolomics study, we quantified the MRSA AIP molecule in the single culture and when this strain was co-culture with commensal strains. The co-culture of *S. simulans* showed inhibition of the MRSA AIP production; however, the MRSA AIP concentration in the co-culture samples of *S. hominis* and *S. warneri* remained unchanged compared to the MRSA single culture. The inhibition of the MRSA AIP molecule in the co-culture of this strain with *S. simulans* shows inhibition of the *agr* system. To track the growth of MRSA, the relative abundance of two molecules that are present in the MRSA strain but not the commensal strains, aureusimine A, and aureusimine B were monitored in the single culture of MRSA and compared to the co-culture samples of *S. simulans.* These results showed that even though the *S.simulans* were inhibiting the MRSA *agr* system, MRSA was still growing in the co-culture samples.

In the untargeted metabolomics study, we detected 5 features using the selectivity ratio model. These molecules showed upregulation or downregulation in the co-culture samples compared to the single culture samples of MRSA and *S. simulans.* These molecules have not been previously identified, and it is essential to identify the role these molecules play in the communication between commensal and pathogenic strains.

REFERENCES

(1)   Parlet, C. P.; Brown, M. M.; Horswill, A. R. Commensal Staphylococci Influence Staphylococcus Aureus Skin Colonization and Disease. *Trends in Microbiology* **2019**, *27* (6), 497–507. https://doi.org/10.1016/j.tim.2019.01.008.

(2)   Byrd, A. L.; Belkaid, Y.; Segre, J. A. The Human Skin Microbiome. *Nature Reviews Microbiology* **2018**, *16* (3), 143–155. https://doi.org/10.1038/nrmicro.2017.157.

(3)   Oh, J.; Byrd, A. L.; Park, M.; Kong, H. H.; Segre, J. A. Temporal Stability of the Human Skin Microbiome. *Cell* **2016**, *165* (4), 854–866. https://doi.org/10.1016/j.cell.2016.04.008.

(4)   Centers for Disease Control and Prevention (U.S.). *Antibiotic Resistance Threats in the United States, 2019*; Centers for Disease Control and Prevention (U.S.), 2019. https://doi.org/10.15620/cdc:82532.

(5)   Ghoul, M.; Mitri, S. The Ecology and Evolution of Microbial Competition. *Trends in Microbiology* **2016**, *24* (10), 833–845. https://doi.org/10.1016/j.tim.2016.06.011.

(6)   Brown, M. M.; Kwiecinski, J. M.; Cruz, L. M.; Shahbandi, A.; Todd, D. A.; Cech, N. B.; Horswill, A. R. Novel Peptide from Commensal *Staphylococcus Simulans* Blocks Methicillin-Resistant *Staphylococcus Aureus* Quorum Sensing and Protects Host Skin from Damage. *Antimicrob Agents Chemother* **2020**, *64* (6), e00172-20, /aac/64/6/AAC.00172-20.atom. https://doi.org/10.1128/AAC.00172-20.

(7)   Iwase, T.; Uehara, Y.; Shinji, H.; Tajima, A.; Seo, H.; Takada, K.; Agata, T.; Mizunoe, Y. Staphylococcus Epidermidis Esp Inhibits Staphylococcus Aureus Biofilm Formation and Nasal Colonization. *Nature* **2010**, *465* (7296), 346–349. https://doi.org/10.1038/nature09074.

(8)   Zipperer, A.; Konnerth, M. C.; Laux, C.; Berscheid, A.; Janek, D.; Weidenmaier, C.; Burian, M.; Schilling, N. A.; Slavetinsky, C.; Marschal, M.; Willmann, M.; Kalbacher, H.; Schittek, B.; Brötz-Oesterhelt, H.; Grond, S.; Peschel, A.; Krismer, B. Human Commensals Producing a Novel Antibiotic Impair Pathogen Colonization. *Nature* **2016**, *535* (7613), 511-516L. http://dx.doi.org/10.1038/nature18634.

(9)   High Frequency and Diversity of Antimicrobial Activities Produced by Nasal Staphylococcus Strains against Bacterial Competitors https://journals.plos.org/plospathogens/article?id=10.1371/journal.ppat.1005812 (accessed Aug 28, 2020).

(10)   Kaur, D. C.; Chate, S. S. Study of Antibiotic Resistance Pattern in Methicillin Resistant Staphylococcus Aureus with Special Reference to Newer Antibiotic. *J Glob Infect Dis* **2015**, *7* (2), 78–84. https://doi.org/10.4103/0974-777X.157245.

(11)   Otto, M. Basis of Virulence in Community-Associated Methicillin-Resistant Staphylococcus Aureus. *Annu. Rev. Microbiol.* **2010**, *64* (1), 143–162. https://doi.org/10.1146/annurev.micro.112408.134309.

(12) DeLeo, F. R.; Otto, M.; Kreiswirth, B. N.; Chambers, H. F. Community-Associated Meticillin-Resistant Staphylococcus Aureus. *The Lancet* **2010**, *375* (9725), 1557–1568. https://doi.org/10.1016/S0140-6736(09)61999-1.

(13) Lyon, G. J.; Novick, R. P. Peptide Signaling in Staphylococcus Aureus and Other Gram-Positive Bacteria. *Peptides* **2004**, *25* (9), 1389–1403. https://doi.org/10.1016/j.peptides.2003.11.026.

(14) Thoendel, M.; Kavanaugh, J. S.; Flack, C. E.; Horswill, A. R. Peptide Signaling in the Staphylococci. *Chem. Rev.* **2011**, *111* (1), 117–151. https://doi.org/10.1021/cr100370n.

(15) Yarwood, J. M.; Schlievert, P. M. Quorum Sensing in Staphylococcus Infections. *Journal of Clinical Investigation; Ann Arbor* **2003**, *112* (11), 1620–1625.

(16) Cheung, G. Y. C.; Wang, R.; Khan, B. A.; Sturdevant, D. E.; Otto, M. Role of the Accessory Gene Regulator Agr in Community-Associated Methicillin-Resistant Staphylococcus Aureus Pathogenesis. *Infection and Immunity* **2011**, *79* (5), 1927–1935. https://doi.org/10.1128/IAI.00046-11.

(17) Paharik, A. E.; Parlet, C. P.; Chung, N.; Todd, D. A.; Rodriguez, E. I.; Van Dyke, M. J.; Cech, N. B.; Horswill, A. R. Coagulase-Negative Staphylococcal Strain Prevents Staphylococcus Aureus Colonization and Skin Infection by Blocking Quorum Sensing. *Cell Host & Microbe* **2017**, *22* (6), 746-756.e5. https://doi.org/10.1016/j.chom.2017.11.001.

(18) Quave, C. L.; Lyles, J. T.; Kavanaugh, J. S.; Nelson, K.; Parlet, C. P.; Crosby, H. A.; Heilmann, K. P.; Horswill, A. R. Castanea Sativa (European Chestnut) Leaf Extracts Rich in Ursene and Oleanene Derivatives Block Staphylococcus Aureus Virulence and Pathogenesis without Detectable Resistance. *PLoS One* **2015**, *10* (8). https://doi.org/10.1371/journal.pone.0136486.

(19) Grundstad, M. L.; Parlet, C. P.; Kwiecinski, J. M.; Kavanaugh, J. S.; Crosby, H. A.; Cho, Y.-S.; Heilmann, K.; Diekema, D. J.; Horswill, A. R. Quorum Sensing, Virulence, and Antibiotic Resistance of USA100 Methicillin-Resistant Staphylococcus Aureus Isolates. *mSphere* **2019**, *4* (4). https://doi.org/10.1128/mSphere.00553-19.

(20) Martínez-García, S.; Ortiz-García, C. I.; Cruz-Aguilar, M.; Zenteno, J. C.; Murrieta-Coxca, J. M.; Pérez-Tapia, S. M.; Rodríguez-Martínez, S.; Cancino-Diaz, M. E.; Cancino-Diaz, J. C. Competition/Antagonism Associations of Biofilm Formation among Staphylococcus Epidermidis Agr Groups I, II, and III. *J Microbiol.* **2019**, *57* (2), 143–153. https://doi.org/10.1007/s12275-019-8322-5.

(21) Anetzberger, C.; Jung, K. Introduction. In *Bacterial Signaling*; John Wiley & Sons, Ltd, 2009; pp 1–5. https://doi.org/10.1002/9783527629237.part1.

(22) Hall, P. R.; Elmore, B. O.; Spang, C. H.; Alexander, S. M.; Manifold-Wheeler, B. C.; Castleman, M. J.; Daly, S. M.; Peterson, M. M.; Sully, E. K.; Femling, J. K.; Otto, M.; Horswill, A. R.; Timmins, G. S.; Gresham, H. D. Nox2 Modification of LDL Is Essential for Optimal Apolipoprotein B-Mediated Control of Agr Type III Staphylococcus Aureus Quorum-Sensing. *PLoS Pathogens* **2013**, *9* (2). http://dx.doi.org/10.1371/journal.ppat.1003166.

(23) Defoirdt, T.; Boon, N.; Bossier, P. Can Bacteria Evolve Resistance to Quorum Sensing Disruption?: E1000989. *PLoS Pathogens* **2010**, *6* (7). http://dx.doi.org/10.1371/journal.ppat.1000989.

(24) Peterson, M. M.; Mack, J. L.; Hall, P. R.; Alsup, A. A.; Alexander, S. M.; Sully, E. K.; Sawires, Y. S.; Cheung, A. L.; Otto, M.; Gresham, H. D. Apolipoprotein B Is an Innate Barrier against Invasive Staphylococcus Aureus Infection. *Cell Host & Microbe* **2008**, *4* (6), 555–566. https://doi.org/10.1016/j.chom.2008.10.001.

(25) Sully, E. K.; Malachowa, N.; Elmore, B. O.; Alexander, S. M.; Femling, J. K.; Gray, B. M.; DeLeo, F. R.; Otto, M.; Cheung, A. L.; Edwards, B. S.; Sklar, L. A.; Horswill, A. R.; Hall, P. R.; Gresham, H. D. Selective Chemical Inhibition of Agr Quorum Sensing in Staphylococcus Aureus Promotes Host Defense with Minimal Impact on Resistance. *PLOS Pathogens* **2014**, *10* (6), e1004174. https://doi.org/10.1371/journal.ppat.1004174.

(26) Todd, D. A.; Zich, D. B.; Ettefagh, K. A.; Kavanaugh, J. S.; Horswill, A. R.; Cech, N. B. Hybrid Quadrupole-Orbitrap Mass Spectrometry for Quantitative Measurement of Quorum Sensing Inhibition. *Journal of Microbiological Methods* **2016**, *127*, 89–94. https://doi.org/10.1016/j.mimet.2016.05.024.

(27) Jones, D. D.; Caesar, L. K.; Pelzer, C. V.; Crandall, W. J.; Jenul, C.; Todd, D. A.; Horswill, A. R.; Cech, N. B. Targeted and Untargeted Analysis of Secondary Metabolites to Monitor Growth and Quorum Sensing Inhibition for Methicillin-Resistant Staphylococcus Aureus (MRSA). *Journal of Microbiological Methods* **2020**, *176*, 106000. https://doi.org/10.1016/j.mimet.2020.106000.

(28) Wyatt, M. A.; Wang, W.; Roux, C. M.; Beasley, F. C.; Heinrichs, D. E.; Dunman, P. M.; Magarvey, N. A. Staphylococcus Aureus Nonribosomal Peptide Secondary Metabolites Regulate Virulence. *Science* **2010**, *329* (5989), 294–296.

(29) Sun, F.; Cho, H.; Jeong, D.-W.; Li, C.; He, C.; Bae, T. Aureusimines in Staphylococcus Aureus Are Not Involved in Virulence. *PLOS ONE* **2010**, *5* (12), e15703. https://doi.org/10.1371/journal.pone.0015703.

(30) Kellogg, J. J.; Todd, D. A.; Egan, J. M.; Raja, H. A.; Oberlies, N. H.; Kvalheim, O. M.; Cech, N. B. Biochemometrics for Natural Products Research: Comparison of Data Analysis Approaches and Application to Identification of Bioactive Compounds. *J. Nat. Prod.* **2016**, *79* (2), 376–386. https://doi.org/10.1021/acs.jnatprod.5b01014.

(31) Ji, G.; Beavis, R. C.; Novick, R. P. Cell Density Control of Staphylococcal Virulence Mediated by an Octapeptide Pheromone. *Proceedings of the National Academy of Sciences of the United States of America* **1995**, *92* (26), 12055–12059.